DIFFERENTIAL OBSERVABLES FOR SOFTWARE-BASED GPS INTERFEROMETRY

B.J. Muth[1,2]*, P.J. Oonincx*[1]*, and C.C.J.M Tiberius*[2]

[1] Faculty of Military Sciences
Netherlands Defense Academy
Het Nieuwe Diep 8, 1780 CA Den Helder, The Netherlands

[2] Department of Earth Observation and Space Systems
Delft University of Technology
Kluyverweg 1, 2629 HS, Delft, The Netherlands

B.J.Muth@tudelft.nl, PJ.Oonincx@nlda.nl, C.C.J.M.Tiberius@tudelft.nl

ABSTRACT

The implementation of an interferometric positioning experiment for measuring the baseline vector between two locations is presented. Two identical software receivers, each consisting of an antenna, a low-cost USB front-end collecting GNSS signals in the L1 band and a laptop, are placed at both ends of the baseline. Cross-correlating the raw signals in post-processing yields differential code delay and carrier frequency observables. A three dimensional baseline vector can be computed after applying corrections to the ranging measurements. Issues related to producing differenced observables, such as the correlation of two noisy signals, the detection and identification of all satellites and issues arising from hardware features of the receivers such as the synchronisation of the two receivers are adressed.

1. INTRODUCTION

Relative positioning with GPS signals originates from the field of interferometry. In this frame two antennas making up for the interferometer baseline vector are used simultaneously to observe one source [1]. When measuring the phase differences of the received signals, the direction of the source can be determined relative to the direction of the baseline vector. The received signals are recorded simultaneously but

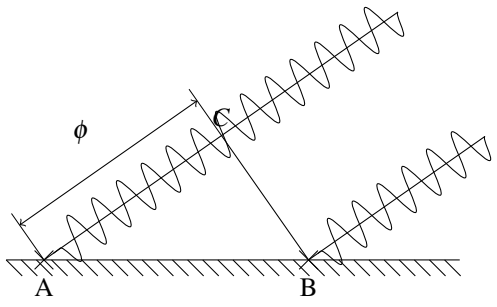

Figure 1: Interferometric configuration considering the plane wave approximation.

independently at the two locations, and later processed to determine the interferometric observables that are of two types: phase observables and group-delay observables. The simplified model of the phase observable ϕ is

$$\phi(t) = \frac{2\pi f}{c}\mathbf{B}(\mathbf{t}).\mathbf{s} + \phi_{media}(t) + \phi_{instru}(t) + 2\pi A \qquad (1)$$

where ϕ is in radians, f is the signal frequency and c the speed of light. In a chosen reference system $\mathbf{B}$ is the baseline vector, $\mathbf{s}$ the unit Line Of Sight vector from the reference point to the source and therefore $\mathbf{B}(\mathbf{t}).\mathbf{s}$ is the projection of the baseline in the direction of the source. Next, $\phi_{media}(t)$ and $\phi_{instru}(t)$ are imprecisions of the observable respectively due to random short-term changes of the media, e.g. multipath, and of the instrumentation, e.g. clock errors. A is the integer number of carrier cycles called the ambiguity. The derivative of the phase ϕ with respect to the angular frequency $2\pi f$ is the interferometric group-delay

$$\tau(t) = \frac{1}{c}\mathbf{B}(\mathbf{t}).\mathbf{s} + \tau_{media}(t) + \tau_{instru}(t) \qquad (2)$$

These phase and group delay observables contain the whole baseline vector information and correspond in the case of GPS respectively to the single-difference carrier phase and code observables. Interferometric positioning, i.e. the computation of a baseline with single-differencing techniques has been achieved first with analog hardware processing GPS signals [2, 3]. The opportunity of having two front-ends for GNSS software receivers has motivated the reproduction of the interferometric experiment in a Software Defined Receiver framework [4]. In that first work the estimation of a baseline vector has been achieved after directly cross-correlating the digitized received signals, producing group-delay, Time-Difference-of-Arrival (TDOA) observables. In this paper we present the implementation of a software-based interferometric positioning experiment using code measurements. In contrast to [4] the direct cross-correlation of the raw IF signals yields for each observation duration a two-dimensional correlation map, from which not only the TDOAs are extracted but also the differential Doppler shift between the satellite signals. Interferometric positioning is a semi-codeless technique, since the structure of the spreading sequences is not needed to produce the observables. This property enables on one hand the processing of signals which code structure is unknown to a particular receiver, e.g. the Chinese GNSS Compass. On the other hand, the knowledge of the spreading codes is necessary in such a setup to demodulate each received satellite signal and to assign satellites PRNs to the interferometric observables before computing the baseline. This is why raw code phase and Doppler estimates are first computed in a standalone mode for all satellites present in a data stream of short duration, before being differenced and matched to the interferometric code and Doppler observables, independently from the interferometric processing and from the synchronisation of the records.

2. INTERFEROMETRY

The baseline vector across two identical software receivers, each consisting of an isotropic antenna, a front-end collecting signals in the L1 band and a laptop, can be computed using group delay and phase observables that are best modeled with equations including terms that account for e.g. atmospheric effects for very precise applications and/or for very long baselines. In our case the differential atmospheric effects can be neglected considering the baseline length. The GNSS signals propagate spherically. The classical plane wave approximation cannot be used since the satellites are too close to the Earth, which results in non-linear observation equations. In the exact spherical case, the deviation from true plane waves is proportional to the square of the baseline length divided by the satellites distances. The linearization is included in the navigation observation equations [1]. Next, accurate reference coordinates available for one station lead to a useable single-difference observation equations. For one observation instant at stations A and B recording signals from the same satellite k, the single-difference phase is modeled as

$$E\left[\Delta p_{AB}^k\right] = \left[\begin{array}{ccc} -\mathbf{e}_B^k & c & \lambda \mathbf{I} \end{array}\right] \left[\begin{array}{c} \Delta \mathbf{x}_{AB}^k \\ \Delta \delta t_{AB} \\ \mathbf{A}_{AB}^k \end{array}\right] \quad (3)$$

where Δp_{AB}^k is the vector of measured phase difference, $\mathbf{e}_B^k$ is the unit LOS vector from station B to satellite k, $\Delta\delta t_{AB}$ the single difference receiver clock error and $\mathbf{A}_{AB}^k$ the single difference ambiguity [6]. This single-difference equation does not contain the satellite clock error, and all other terms make up for differences between the receivers, or between the reference receiver and the satellite. The single difference equation for code observables ΔP_{AB}^k is similar the equation above, minus the ambiguity terms

$$E\left[\Delta P_{AB}^k\right] = \left[\begin{array}{cc} -\mathbf{e}_B^k & c \end{array}\right] \left[\begin{array}{c} \Delta \mathbf{x}_{AB}^k \\ \Delta \delta t_{AB} \end{array}\right] \quad (4)$$

The single difference phase equation (3) is rank deficient. Amiguities can be fixed by using double-differences, i.e. differences between satellites. Ambiguities could be left floating, though the standard deviation of the baseline precision computed with phase observables collected during less than one minute would be higher than the baseline precision obtained with pseudoranges observables. In other words, with our material that enables maximal recording durations of 38 seconds, fixing the ambiguities is necessary to fully take advantage of the precision of the carrier phase measurements. In the double difference equation the ambiguities are integer-valued which helps solving for them [5].

3. SIGNAL

GPS L1 C/A signals have been recorded simultaneously at two stations located respectively at (52°57'5.0866" N, 4°43'16.4121" E) and (52°53'20.8461" N, 4°51'0.1637") near Den Helder, The Netherlands, with the front-ends described below. The recordings have been performed during 38 seconds every 3 minutes. The signal received in A from satellite k writes

$$s_A^k[n] = a_k\,(c^k.d^k)(nT_s - \tau^k)\cos(2\pi f_{IF} n T_s + \phi^k) \quad (5)$$

where a^k is the amplitude of the signal in volts, c^k is the binary PRN code sequence and d^k the binary data sequence. n is the sampling index and T_s the sampling period in seconds. ϕ^k is the carrier phase in radians including the carrier Doppler shift seen from the receiver $f_{d,L1}^k$ in Hertz, and the signal travel-time τ^k in seconds. The signal received from K satellites at station A writes $s_A[n] = \sum_{k=1}^{K} s_A^k[n] + \varepsilon[n]$ where ε is an additional white Gaussian noise process. At both stations the raw data have been recorded with the Sparkfun GN3S front-end module [8] built for the Danish GPS Center SoftGPS project and accompanying the book [7]. This low-cost front-end includes a magnetic patch antenna and a SiGe SE4110L GPS chip. The receiver bandwidth is 2.2 MHz wide and the analog part downconverts the signal to an intermediate frequency f_{IF} of 4.1304 MHz. The analog-to-digital converter produces f_s equal to 16.3676 Msamples/sec and quantizes the signal with 2 bits. The front-end is connected to a laptop through a USB connection. Only a driver is needed to have a functioning receiver, however this driver limits the recording duration to 38 seconds.

The signal model (5) is used for the interferometric processing we set up in Sections 4 to 6 and that is meant to produce the interferometric observables. The same model is used for the open-loop standalone processing set up in Section 7.1, which is meant to identify these observables . This signal model is also used for the closed-loop standalone processing in Section 7.2 that originates from [7]. This step is meant to produce the navigation data in a classical way for both records, cross-correlate these data streams and obtain a time offset used to slide the records before the interferometric processing, achieving the synchronisation of the receivers.

4. CORRELATION

Assuming the receivers are synchronised, the cross-correlation function (CCF) of the two collected signals yields a correlation map featuring peaks that represent localized versions of the individual CCF of all received satellite signals present in the two streams. These peaks can be best described by the auto-correlation function (ACF) of the transmitted GPS signal, which in turn can be approximated to the ACF of its one millisecond periodic PRN spreading code. The ACF of the code sequence can be written as

$$R(\tau, f) = \Lambda_{T_c}(\tau)\mathrm{sinc}(\pi \mathrm{f} \mathrm{T_c}) \quad (6)$$

where $\Lambda_T = 1 - |\tau|/T$ for $|\tau| \leq T$ is the triangle function of width T, $\mathrm{sinc(u)} = \sin(\mathrm{u})/\mathrm{u}$ is the sine cardinal function and T_c is one chip length. Next, considering sequences of discrete signal samples, one possible definition of the sampled CCF writes according to [9]

$$\hat{c}_{AB}[m] = \frac{1}{N_p} \sum_{n=0}^{N_p - |m| - 1} s_A[n] s_B[n - |m|] \qquad m \geq 0 \quad (7)$$

where N_p is the length of signals s_A and s_B. Besides the differential code phase, we also need to compute the differential Doppler frequency. Differential frequency bins are then introduced and the correlation $c_{AB}[m, f]$ is computed iteratively as illustrated in Figure 2, where f is the shift on the signal s_B. Considering the baseline length in our example and the

computational cost of the correlation, an irregular frequency grid having more samples in the region around the IF frequency is chosen. The correlation c of one millisecond of data collected at stations A and B writes

$$c(\tau_{AB}, f^d_{AB}) = s_A(t,f) \odot s_B(t+\tau_{AB}, f+f^d_{AB}) \qquad (8)$$

with $\odot$ the circular correlation using the FFT operation [7]. The cross-correlation of two noisy GPS signals has a SNR

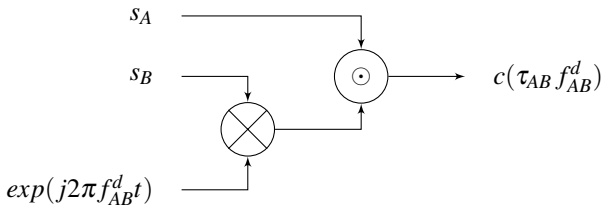

Figure 2: Correlation and integration at f_{IF}.

roughly 30 dB lower than the cross-correlation of one received GPS signal and a clean replica [1]. In order to detect the energy from the satellites, the correlation has to be integrated over several code periods. Coherent integration durations of 250 milliseconds, respectively 1000 milliseconds, have been chosen in [3], and [2]. The performance of coherent integration is a topic of further research, and the sampled CCF is here integrated non-coherently during $N_{NC} = 1000$ code periods

$$C(\tau_{AB}, f^d_{AB}) = \frac{1}{N_{NC}} \sum_{m=1}^{N_{NC}} \left| c(\tau_{AB}, f^d_{AB}) \right|^2 \qquad (9)$$

The cross-correlation of two frequency-shifted versions of the signals then yields a two-dimensional correlation map that contains all the information related to the TDOA and differential Doppler of the signals received at the two stations.

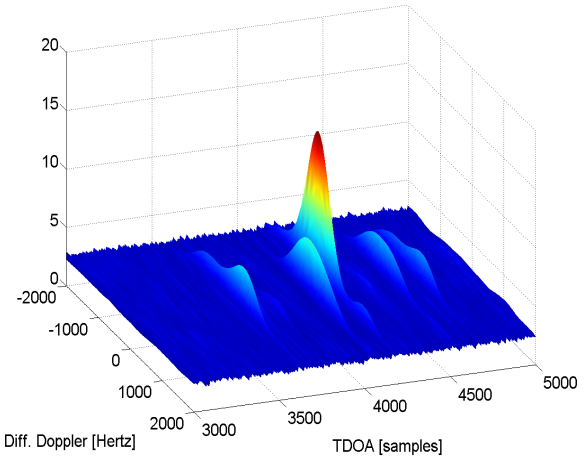

Figure 3: Correlation map obtained for an observation duration of one second.

5. DETECTION

The integrated CCF obtained from one observation duration is illustrated on Figure 3. This map shows several peaks localised in time and frequency that correspond to the cross-correlation between the various satellite signals. Outside the peaks region the correlation surface can be considered as almost flat. The average noise floor, therefore the detection threshold considered for the detection over all observation durations, are computed from the statistics of the correlation values. For each observation duration, the detection proceeds as depicted in Figure 4. The maximum γ of the correlation map C is sought. If the computed maximum γ is superior to the noise floor γ_0, the parameters maximising the correlation map are the estimated differential code delay and Doppler, and the rectangular region Ω of the correlation map of width 3 chips and all differential Doppler bins around the detected peak is removed from the correlation map. Otherwise the search moves on to the next observation duration.

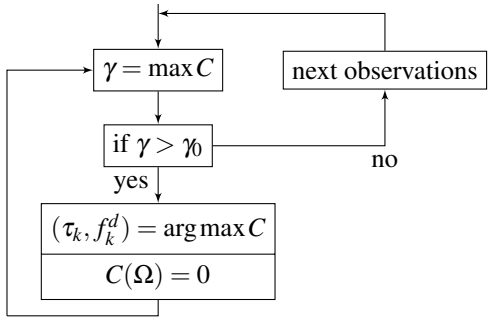

Figure 4: Detection operation after one observation duration.

6. MEASUREMENTS

The resolution of the differential code phase and differential Doppler measurements is limited by the dimensions of the correlation map, which is in turn conditioned by the computational cost of the correlation operations and the computer's memory. On one hand the sampling frequency drives the time resolution of the code phase observables. On the other hand the frequency resolution of the observables is chosen in an arbitrary manner, i.e. as fine as one wants. The refinement of the observables then consists in taking the estimated frequency bin and interpolating the correlation values in that bin. This results in new TDOA estimates having a higher resolution than one time sample. While the TDOA measurements can directly be extracted from the correlation map, the production of differential phase observables is more difficult. Indeed the phase alignment between the data streams cannot be computed from the cross-correlation of the signals without an external phase reference and the knowledge of the code alignment. Next if a phase measurement is obtained, its accuracy is not guaranteed with our hardware.

7. IDENTIFICATION

7.1 Satellites

The satellites were identified in [4] using a matching of the individual acquisition metrics with the amplitude of the

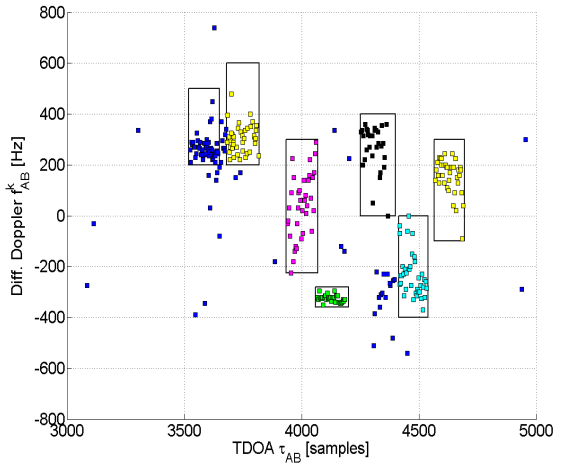

Figure 5: Differential code-Doppler observables obtained from 37 observation durations of one second each.

cross-correlation peaks. This method is not reliable due to several phenomena, the most obvious being the difference in the recording environments. Figure 5 depicts clusters of corrected interferometric observables, that correspond to visible but unknown satellites we identify thanks to their differential Doppler. Indeed the code phase-Doppler shift parameters of the detected satellites can be computed separately for each data record during less than 10 seconds, with an open-loop processing illustrated in Figure 6. This sequential pro-

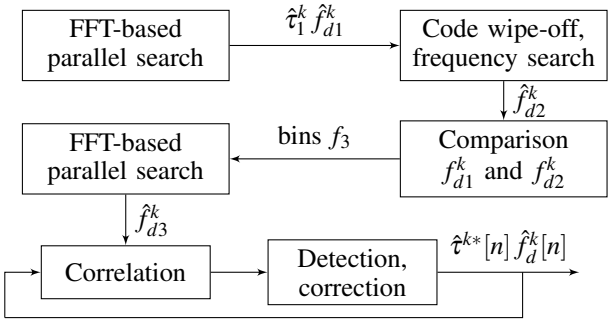

Figure 6: Standalone open-loop processing for producing code phase and Doppler observables.

cessing is preceded by a FFT-based parallel search meant to achieve a code and carrier acquisition with first coarse frequency estimates $\hat{f}^k_{d1}$, then increasingly fine frequency estimates $\hat{f}^k_{d1}$, $\hat{f}^k_{d2}$ and $\hat{f}^k_{d3}$. Non-coherent integration durations of 10 code periods are used to increase the sensitivity of the reception. The sequential processing itself also uses integration, though with shorter durations, and yields estimates for the code phase $\hat{\tau}^k[n]$ and the Doppler $\hat{f}^k_d[n]$ at each recursion. Given the nominal value of the sampling frequency (see Section 3), the number of samples per code period has to be rounded. One correction is applied to compensate for the non-integer number of samples per code period and for the code Doppler shift, resulting in the new code phase

$$\hat{\tau}^{k*}[n] = \left(\frac{16.3676}{16.368}\right)\left(\frac{f_{L1}}{f_{L1}+f^k_d[n]}\right)\hat{\tau}^k[n] \qquad (10)$$

The strongest satellites in each data record were kept and those obviously not being able to lock discarded. Collecting the code phase and Doppler information for all satellites yields maps for each of the raw data streams, which are then differenced modulo one code period. These differenced observables having known PRN are illustrated in Figure 7, providing a reference map for the interferometric observables displayed in Figure 5. The matching between the two maps should only be a matter of geometry or shape, not of numerical values, indeed the observables should only be precise enough to discriminate different satellites within a map.

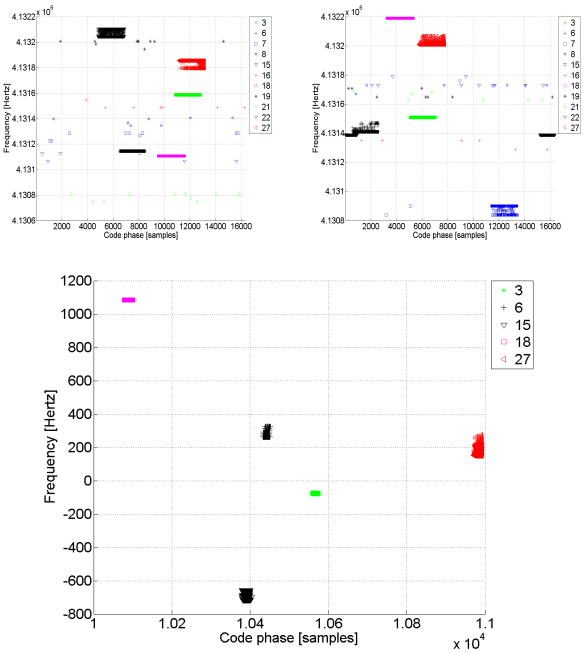

Figure 7: Code-Doppler results from the standalone processing at the two stations (up) and differenced results for the strongest satellites (below) that is used as a reference for identifying the interferometric observables.

7.2 Clocks

Each receiver is based on two clocks: the front-end crystal oscillator and the laptop clock from which a time-tag is produced for each signal file. Both laptop clocks were synchronised via a LAN connection to a time server shortly before the experiment. However, this synchronisation is not accurate enough. Next, all clocks drift which creates an extra difficulty for synchronisation. This issue is then tackled in two steps. First, a coarse synchronisation of the records start is achieved by cross-correlating the navigation data obtained from the separate demodulation of the two signals received from one satellite. This demodulation uses extended non-coherent integration for acquisition and coupled DLL/PLL tracking loops that are configured as in the software accompanying [7], yielding the 1 kHz-sampled GPS navigation data

and contained in the in-phase prompt (I_P) correlator outputs. Assuming two such data streams are long enough to contain common data bits, their cross-correlation depicted in Figure 8, then yields a coarse clock offset which is used to slide the records before the interferometric cross-correlation. This coarse adjustment is necessary to cross-correlate signal streams having similar data bits, achieve maximal correlation and detect the different signals. Even if the computed clock offset has more reliability when the adjustment is repeated for several satellites, it has a 1 ms resolution that is not accurate enough, and it masks the true differential delay due to the satellite and baseline geometry. Depending on the baseline length, this true TDOA can be neglected compared to the clock offset computed with this method of data cross-correlation. Though in all cases, a residual differential clock error remains after the synchronisation given the resolution issue mentioned above. This residual offset is eventually estimated with more precision together with the baseline itself as shown in the observation equations from Section 2. The coarse differential clock offset is computed by cross-

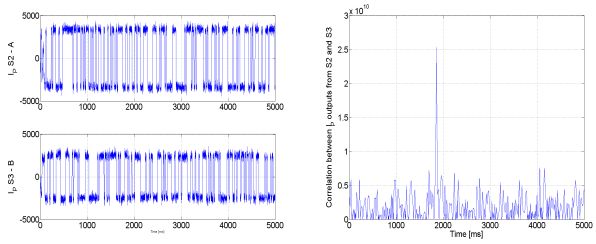

Figure 8: In-phase prompt correlation outputs at the two stations (left) and coarse estimated time-delay between the start of the records, resolution of one code period (right).

correlating the demodulated navigation data obtained from all pairs of signals recorded during the campaign. This offset is illustrated in Figure 9 and shows a significant change in amplitude that reaches a maximum value in the order of magnitude of 1 second per 10 minutes. This testifies of the instability of the receiver clocks when put together in our interferometric setup.

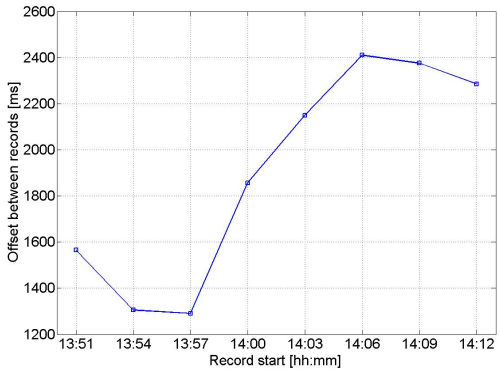

Figure 9: Differential clock offset for all signals recorded during the measurement campaign.

8. CONCLUSION

In this paper we presented a methodology to produce and identify differential code measurements for GNSS interferometry, and processing results obtained with this methodology after collecting real data in the field. GNSS interferometry is a semi-codeless concept that has been shortly introduced before presenting the obtention of differential code and carrier observables and their processing for positioning purposes. Based on the GPS L1 C/A signal definition, the cross-correlation map resulting from the integration is modeled. Methods for taking care of the synchronisation between the start of the records, and for identifying the satellites using the standalone processing of the data collected at the two stations have been presented. Concerning the processing of code measurements, further research regards the trade-off between coherent and non-coherent integration, its impact on the localisation of the energy and the detection. However the biggest challenge is the creation and processing of phase measurements that leads in theory to a better baseline precision. The experiment setup we present provides a good benchmark for this purpose, though achieving this challenge is questionable given the characteristics of the low-cost hardware in our possession.

Acknowledgements

Student officers Borsboom, Hilst and Woudstra have to be thanked for their help.

REFERENCES

[1] G. Seeber, *Satellite Geodesy*, “de Gruyter,” Second edition, 2003.

[2] C. C. Counselman and I. I. Shapiro, “Miniature interferometer terminals for earth surveying,” *Journal of Geodesy*, vol. 53, pp. 139–163, 1979.

[3] P. F. MacDoran, “Satellite Emission Radio Interferometric Earth Surveying Series - GPS Geodetic System,” *Bull. Geod.*, pp. 117–138, 1979.

[4] B. J. Muth, “Software-based GNSS L1 Interferometric Positioning,” in *Proc. of the 21th ION GNSS Conf.*, 2008.

[5] P. J. G. Teunissen, “Least-squares estimation of the integer GPS ambiguities,” in *Invited Lecture. Section IV Theory and Methodology, IAG General Meeting, Beijing, China*. August 1993.

[6] P. Misra and P. Enge, *Global Positioning System: Signals, Measurements, and Performance*, Ganga-Jamuna Press, 2006.

[7] D. Akos and K. Borre, *A single-frequency software-defined GNSS receiver*, Birkhaueser, 2006.

[8] Sparkfun Electronics, http://www.sparkfun.com

[9] M. B. Priestley, *Spectral Analysis and Time Series*, Academic Press, Ninth edition, 1996.

[10] B.R. Townsend and P. Fenton, “A practical approach to the reduction of pseudorange multipath errors in a L1 GPS receiver,” in *Proc. of the IEEE Position Location and Navigation Symposium (PLANS 94)*, vol. 1, pp. 246-251, Salt Lake City, Utah, USA, Sept. 1994.